Received: 27 June 2020 | Revised: 8 July 2020 | Accepted: 8 July 2020

DOI: 10.1002/cey2.70

RESEARCH ARTICLE

CARBON ENERGY WILEY

The electrolyte comprising more robust water and superhalides transforms Zn-metal anode reversibly and dendrite-free

Chong Zhang[1,2] | **Woochul Shin**[2] | **Liangdong Zhu**[2] | **Cheng Chen**[2] | **Joerg C. Neuefeind**[3] | **Yunkai Xu**[2] | **Sarah I. Allec**[4] | **Cong Liu**[5] | **Zhixuan Wei**[2] | **Aigerim Daniyar**[2] | **Jia-Xing Jiang**[1] | **Chong Fang**[2] | **P. Alex Greaney**[4] | **Xiulei Ji**[2]

[1]Key Laboratory of Applied Surface and Colloid Chemistry (Shaanxi Normal University), Ministry of Education, Shaanxi Key Laboratory for Advanced Energy Devices, School of Materials Science and Engineering, Shaanxi Normal University, Xi'an, Shaanxi, China

[2]Department of Chemistry, Oregon State University, Corvallis, Oregon

[3]Spallation Neutron Source, Oak Ridge National Laboratory, Oak Ridge, Tennessee

[4]Materials Science and Engineering, University of California, Riverside, California

[5]Argonne National Laboratory, Chemical Sciences and Engineering Division, Lemont, Illinois

Correspondence
Jia-Xing Jiang, Key Laboratory of Applied Surface and Colloid Chemistry (Shaanxi Normal University), Ministry of Education, Shaanxi Key Laboratory for Advanced Energy Devices, School of Materials Science and Engineering, Shaanxi Normal University, Xi'an, Shaanxi 710062, China.
Email: jiaxing@snnu.edu.cn

Chong Fang and Xiulei Ji, Department of Chemistry, Oregon State University, Corvallis, OR 97331-4003.
Email: Chong.Fang@oregonstate.edu (CF) and david.ji@oregonstate.edu (XJ)

P. Alex Greaney, Materials Science and Engineering, University of California, Riverside, CA 92521.
Email: agreaney@engr.ucr.edu

Funding information
China Scholarship Council, Grant/Award Number: 201706870033; Oregon State University for AID program; National Natural Science Foundation of China, Grant/Award Number: 21574077 & 21304055; U.S. National Science Foundation: CHE-1455353 & DMR-1920368

Abstract

A great challenge for all aqueous batteries, including Zn-metal batteries, is the parasitic hydrogen evolution reaction on the low-potential anode. Herein, we report the formula of a highly concentrated aqueous electrolyte that mitigates hydrogen evolution by transforming water molecules more inert. The electrolyte comprises primarily $ZnCl_2$ and LiCl as an additive, both of which are inexpensive salts. The O–H covalent bonds in water get strengthened in a chemical environment that has fewer hydrogen bonding interactions and a greater number of Zn–Cl superhalides, as suggested by integrated characterization and simulation. As a result, the average Coulombic efficiency of zinc-metal anode is raised to an unprecedented >99.7% at 1 mA cm^{-2}. In the new electrolyte, the plating/stripping processes leave the zinc-metal anode dendrite-free, and the zinc-metal anode delivers stable plating/stripping cycles for 4000 hours with an areal capacity of 4 mAh cm^{-2} at 2 mA cm^{-2}. Furthermore, the high Coulombic efficiency of zinc-metal anode in the $ZnCl_2$-LiCl mixture electrolyte is demonstrated in full cells with a limited anode. The $V_2O_5{\cdot}H_2O$||Zn full cell with an *N*/*P* mass ratio of 1.2 delivers a stable life of more than 2500 cycles, and the $LiMn_2O_4$||Zn hybrid cell with an *N*/*P* mass ratio of 0.6 exhibits 1500 cycles in its stable life.

KEYWORDS

LiCl, reversibility, stability, water-in-salt electrolyte, Zn anode, $ZnCl_2$

1 | INTRODUCTION

The global energy storage installation is predicted to grow by more than 10-fold by 2040. Aqueous Zn-metal batteries (ZMBs) are safe, environmentally benign, and potentially offer an energy density only second to Li-ion batteries.[1,2] Importantly, for achieving a global scale up, zinc as a commodity metal is advantageous. Its global production was around 13.5 million metric tons in 2019, where a fraction of that, ca. 30%, may suffice the 2040's entire global energy storage needs through ZMBs. ZMBs may deliver its stored energy at a competitive levelized energy cost. However, almost all commercial Zn-metal batteries are non-rechargeable, including the alkaline primary batteries and Zn-air primary batteries for hearing aids. Despite the remarkable progress made on high-performing cathode materials,[1-10] the showstopper of ZMBs is the poor reversibility of zinc-metal anode (ZMA) in aqueous electrolytes.[11] ZMA suffers from low Coulombic efficiency (CE) and dendrite formation, common problems for metal batteries, including Li-metal batteries. A low CE means that not all of the Zn stripped from the anode during discharge is replated back during charging for the next use. Therefore, excessive ZMA has to be used to compensate for its piecemeal loss in every cycle so that a meaningful cycle life can be achieved. To promote the reversibility of ZMA, one consideration is to eliminate dendrites first, for example, by using 3D current collectors,[12-15] the current collectors with a low lattice mismatch for Zn,[16] interfacial layers[17-21] or controlling the crystallographic orientations of Zn anode by electrodeposition.[22] Another approach is to restrain the potential drop at the beginning of Zn deposition.[23] Recently, an efficient method was reported to enhance the reversibility of the Zn anode by introducing a solid electrolyte interphase (SEI) particularly via water-in-salt electrolytes (WiSE).[11]

We deem that the root cause of ZMA's irreversibility is its parasitic reaction with water, leading to H_2 evolution.[11,14] To mitigate Zn/H_2O reactivity, one should enhance water's cathodic stability and zinc's anodic stability. In WiSE, H_2O molecules are "captured" by a swarm of cations and anions, which decreases the local activity of water and improves ZMA's reversibility.[24] Unfortunately, the correlation between hydrogen evolution and the chemical environment of water in the electrolytes remains elusive.

Herein, we report that the addition of LiCl into a $ZnCl_2$ WiSE transforms the chemical environment of water such that the hydrogen bonding network of water is further interrupted, the O–H covalent bonds in water are better strengthened, and unprecedented reversibility and stability of ZMA are demonstrated. In the $ZnCl_2$-LiCl WiSE, the completely dendrite-free ZMA delivers an ultrahigh average CE of 99.7% at 1 mA cm^{-2}. With an areal capacity of 4 mAh cm^{-2}, the Zn||Zn symmetric cells last for over 1000 cycles, that is, 4000 hours. In addition, limited ZMA in full cells demonstrates high reversibility in the $ZnCl_2$/LiCl mixture electrolyte. Our results show that it is viable to enable a highly reversible ZMA by transforming the thermodynamics of water and ZMA by engineering their chemical environments without kinetic controls such as SEI.

2 | RESULTS AND DISCUSSIONS

2.1 | Reversibility of ZMA in LiCl-$ZnCl_2$ WiSE

Usually aqueous electrolytes that contain the number of water molecules comparable with the solvated ions are referred to as WiSE (Figure 1A). For $ZnCl_2$ WiSE, as the anion is mostly $[ZnCl_4]^{2-}$, a water/$ZnCl_2$ molar ratio of 3 is sufficient to form a $ZnCl_2$ WiSE theoretically without free water molecules, when assuming the complex cation is $[Zn(OH_2)_6]^{2+}$. In 30 m $ZnCl_2$ WiSE, where the mass and molar ratio of water to $ZnCl_2$ are only 0.24 and 1.85, respectively, the average hydrated Zn^{2+} ions are $[Zn(OH_2)_{3.7}]^{2+}$. After adding LiCl into 30 m $ZnCl_2$ WiSE, the hydration shells of Zn^{2+} must be further downsized. Interestingly, the initial addition of LiCl decreases the viscosity of the resulting WiSE and increases the conductivity (Figures 1B and S1). To refer to these $ZnCl_2$-based WiSEs, the pure 30 m $ZnCl_2$ and the $ZnCl_2$-LiCl mixture electrolytes are named as 30ZC and 30ZC*n*LC, respectively, where *n* denotes the molality of LiCl. For example, we refer to the mixture electrolyte of 30 m $ZnCl_2$ plus 5 m LiCl as 30ZC5LC.

The average CE for ZMA plating/stripping was investigated with galvanostatic charge/discharge (GCD) measurements in asymmetrical Ti||Zn cells with Ag/AgCl in a 4.8M KCl solution as the reference electrode. The measurements for the average CE of ZMA were conducted by following the well-established method by Zhang and colleagues, which has been widely applied for Li-metal anode.[25]

As for the tests for average CE, at first, a complete plating/stripping cycle at the capacity of 4 mAh cm^{-2} was conducted to condition the current collector of Ti foil to reduce oxidant impurities on the substrate surface. Then, a given quantity of charges, that is, Q_T, 4 mAh cm^{-2}, were deposited as the initial Zn active mass on the Ti foil. Next, a smaller capacity, that is, Q_C, 0.4 mAh cm^{-2}, was used to repetitively strip/plate Zn mass from/onto the mass initially deposited on the Ti foil as the working electrode for 100 cycles, where a Zn foil was used as the counter/reference electrode. After 100 cycles, the residue of ZMA was exhaustively stripped to the cut-off potential,

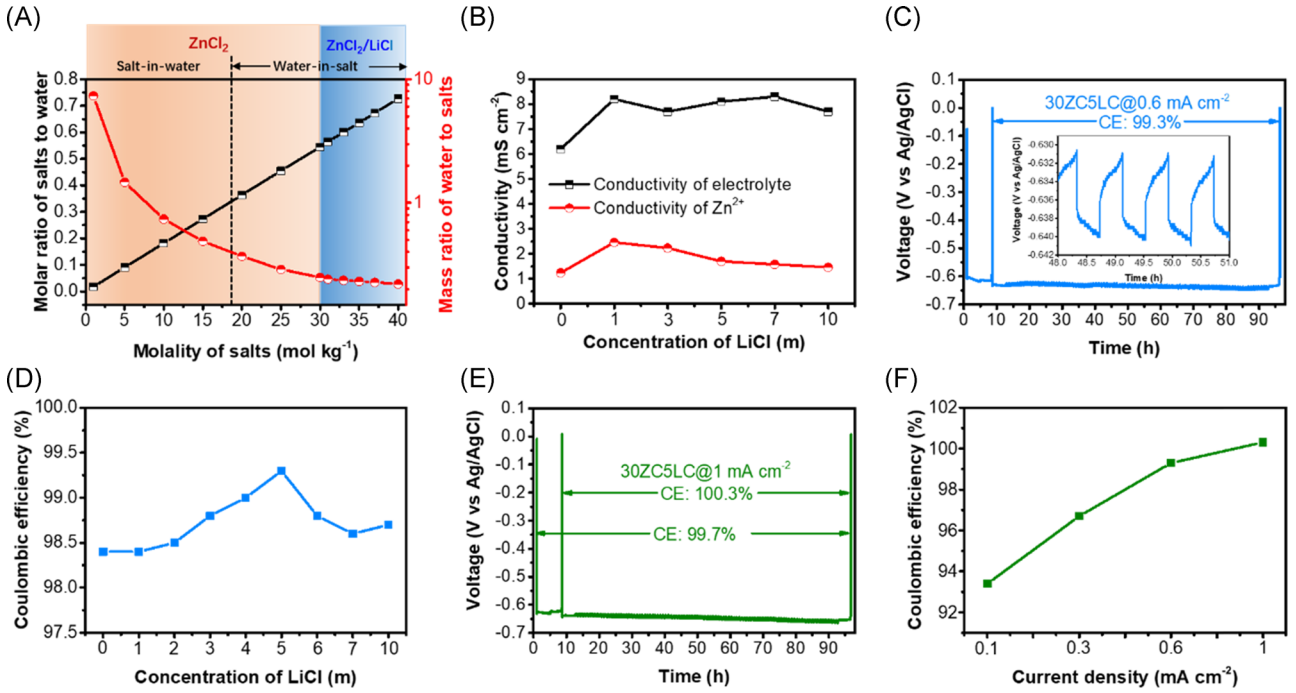

FIGURE 1 Properties of the electrolytes and the reversibility of zinc-metal anode. A, The concentration of salts as a function of the mass and molar ratio between $ZnCl_2$/LiCl and H_2O. B, The conductivity of electrolytes and Zn^{2+} for $ZnCl_2$-LiCl water-in-salt electrolytes (WiSE) with varying LiCl concentrations. The conductivity of Zn^{2+} is the product of the electrolyte conductivity and the transference number of Zn^{2+}. C, The galvanostatic charge/discharge (GCD) potential profiles for the Coulombic efficiency (CE) measurements in 30ZC5LC at 0.6 mA cm^{-2}. D, The CE tests for Zn plating/stripping at 0.6 mA cm^{-2} in $ZnCl_2$-LiCl mixture WiSEs with different LiCl concentrations. E, The GCD profiles at 1 mA cm^{-2} for the CE measurements in 30ZC5LC WiSE. F, The CE results for Zn plating/stripping in 30ZC5LC at different current densities

obtaining the final stripping capacity of Q_S. Thus, the average CE can be calculated by:

$$CE_{avg} = (100\,Q_C + Q_S)/(100\,Q_C + Q_T). \quad (1)$$

This average CE test resembles the cycling process of ZMA in full cells because in full cells, the capacity ratio between the ZMA and the cathode is above 1, ZMA being excessive, which is necessary for all metal batteries due to the less-than-six-sigma efficiencies of metal anodes. Such tests in the authors' opinion are more informative than a test where the plated metal anode is completely stripped in every cycle. As an important factor, the latter test does not involve the parasitic reactions between the idle mass of the metal anode with electrolytes, which is of less harsh conditions.

Recently, we have used this method for other metal electrodes than lithium, including ZMA and Fe-metal anode.[24,26] Figure 1C,D shows the average CE of ZMA at 0.6 mA cm^{-2} in different electrolytes. The plating/stripping processes of ZMA in the $ZnCl_2$-LiCl mixture electrolytes exhibit higher CE values than that in the pure 30 m $ZnCl_2$ electrolyte, which suggests that the presence of LiCl helps suppress H_2 evolution. Interestingly, the CE of Zn plating/stripping in the $ZnCl_2$-LiCl mixture WiSE increases first and then slightly decreases upon increasing the LiCl concentration. The value of CE reaches its maximum of 99.3% when adding 5 m LiCl into the 30 m $ZnCl_2$ electrolyte (forming 30ZC5LC), compared with 98.4% in the 30ZC electrolyte and 98.7% in 30ZC10LC, which is to be discussed *vide infra*.

It is worth noting that the applied current density affects the measured CE of ZMA, as shown in Figures 1C,D and S2. In 30ZC5LC, the CE increases from 93.4% to 100.3% with the current density increasing from 0.1 to 1 mA cm^{-2}. This phenomenon, also reported by other studies,[14,27,28] highlights the fact that a high current rate can dwarf the impacts of hydrogen evolution reaction (HER) on CE of ZMA. Note that in practical cells, if we assume the mass loading on the cathode is 20 mg cm^{-2} and the cathode's specific capacity is 150 mAh g^{-1}, a 1 C rate corresponds to 3 mA cm^{-2}, where 1 mA cm^{-2} often used in the literature for testing the CE of ZMA is C/3 here, thus still being practically relevant. However, to reveal the kinetics of HER in electrolytes, a lower current rate of 0.1 mA cm^{-2}, for example, that is, C/30 for the above hypothetical full cell, can be used to separate stellar electrolytes from good ones. As far as we know, there are very few CE tests on ZMA reported that were

conducted at 0.1 mA cm^{-2} or lower rates. The research community of ZMA is in urgent need of standardized tests to compare CE values. For the business of ZMA, the superlative CE of ZMA obtained at extremely high current densities, for example, 10 mA cm^{-2}, can be misleading because such tests bear no interests in knowing how fast water reacts with ZMA.

Usually, in studies of CE of metal anodes, the initial conditioning cycle(s) that typically suffers low reversibility of plating/stripping are not considered when calculating CE, where these cycles are deemed as a "cleansing" process. However, these initial cycles might leave some stranded metal mass, which may be reclaimed in later cycles, thus rendering the CE of metal anode overestimated. In this study, the CE more than 100% at 1 mA cm^{-2} perhaps exemplifies such a scenario. However, the CE at around 100% demonstrates that 30ZC5LC has pushed the reversibility of ZMA plating-stripping to the limits. If we include the CE of 93.2% from the first "cleansing" cycle in the calculation, the average CE of ZMA still reaches an ultrahigh value of 99.7% at 1 mA cm^{-2} in 30ZC5LC. For comparison, the CE measured in the mixture WiSE of 21 m LiTFSI/1 m $Zn(TFSI)_2$ is less than 75% in the first cycle due to the SEI formation, which quickly rises to 99.2% in the second cycle, and it was stabilized to 99.7% in the following cycles.[11] Therein, the average CE with the trifluoromethanesulfonimide (TFSI)-based WiSE may be slightly less than 99.7%. Though not comparable directly, the ZMA's reversibility in 30ZC5LC is among the most competitive (see Table S1).

We characterized how the addition of LiCl affects the atomic structure of $ZnCl_2$ WiSE by a suite of tools, including femtosecond stimulated Raman spectroscopy (FSRS), Fourier-transform infrared spectroscopy (FTIR), and pair distribution function (PDF) studies associated with the neutron total scattering.

As a sensitive spectroscopic tool with ultrafast laser pulses, FSRS can capture molecular vibrational motions and reveal much of the chemical bonds in WiSEs by elucidating the coordination shells of the Zn^{2+} ions in the low-frequency region (<500 cm^{-1}) and the O–H stretches of water in the high-frequency region (>3000 cm^{-1}). Figures 2A,B and S3a,b show stimulated Raman (ground state FSRS) spectra in the low-frequency region, where the peaks at ~380, 337, 293, and 240 cm^{-1} are attributed to the Zn–O vibrations in $[Zn(OH_2)_6]^{2+}$, and Zn–Cl vibrations in superhalides (we refer to all Zn–Cl complex ions here as superhalides for simplicity) of $[ZnCl_3(OH_2)]^-$ and $[ZnCl_4]^{2-}$, and polynuclear aggregates of $[ZnCl_4]^{2-}$ bridged by Cl atoms, respectively.[29-32] By increasing the LiCl concentration, the peak intensities of Zn–O in $[Zn(OH_2)_6]^{2+}$ and Zn–Cl vibrations in $[ZnCl_3(OH_2)]^-$ decrease, whereas the intensity of Zn–Cl vibrations in the polynuclear aggregates increases. Therefore, LiCl in the WiSE plays dual roles, providing Li-ions to compete against Zn^{2+} for the available H_2O as ligands, and providing additional chloride ions to further extract Zn^{2+} from cationic $[Zn(OH_2)_6]^{2+}$ in forming more superhalide anions.[33]

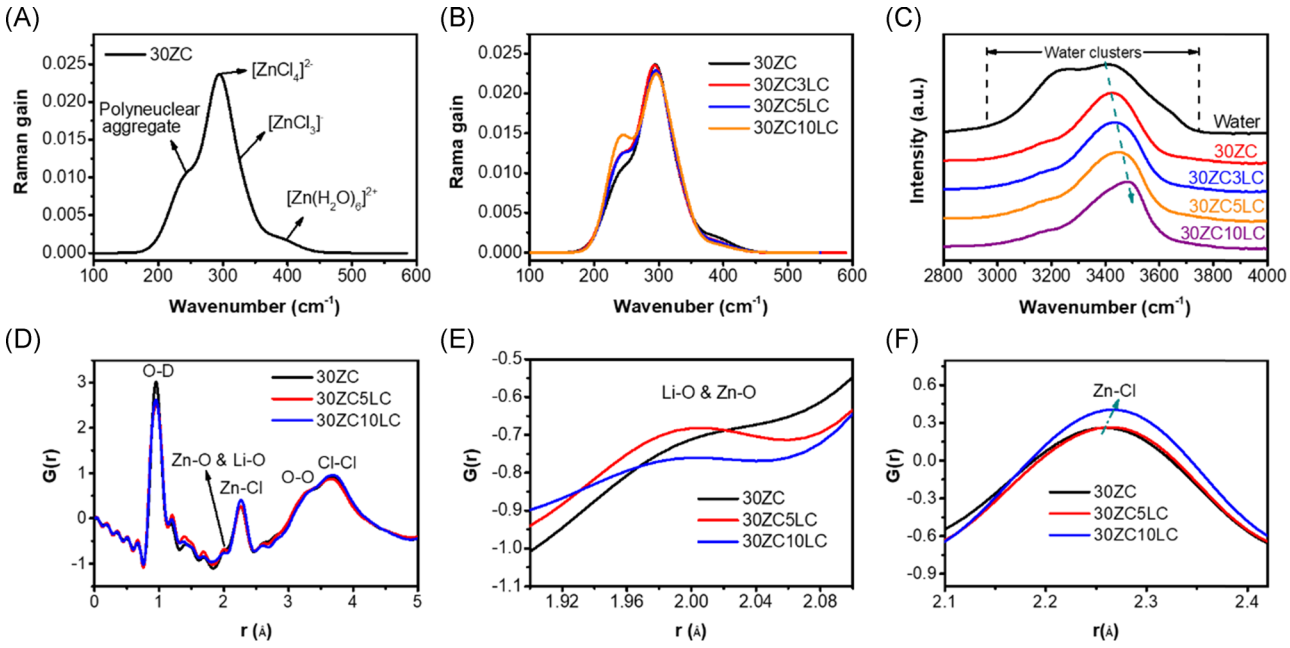

FIGURE 2 Characterization of the atomic structure in $ZnCl_2$-based water-in-salt electrolyte (WiSE). A and B, FSRS spectra of the $ZnCl_2$/LiCl mixture electrolytes in the low-frequency region. C, FSRS spectra in the high-frequency region. D, E, and F, PDF profiles associated with neutron total scattering of 30ZC, 30ZC5LC, and 30ZC10LC WiSE

Figure 2C shows the stimulated Raman spectra for the $ZnCl_2$-based WiSEs and pure water in the high-frequency region. For pure water, its H-bond network mainly consists of two O–H environments: more H-bonded and less H-bonded, attributed to the O–H bond stretching vibrations at ~3230 and 3420 cm^{-1}, respectively. Nevertheless, in the 30 m $ZnCl_2$ WiSE, the O–H stretch only exhibits one dominant peak at ~3454 cm^{-1} without the redder peak, indicating that the chemical environment of water molecules becomes homogenized in the presence of a large amount of ions in WiSE, and fewer water molecules can adjoin each other to form H-bonds. Moreover, the O–H bonds of non-H–bonded water become stiffer in the presence of 30 m $ZnCl_2$. Furthermore, we observed that upon adding the LiCl co-salt, the O–H stretching mode further blueshifts from 3454 cm^{-1} in 30ZC to 3481 cm^{-1} in 30ZC10LC electrolyte.

However, it had been usually expected that the binding between a strong Lewis acid, for example, Zn^{2+} and the oxygen-end of water would weaken the O–H bond, thus causing the O–H vibration to redshift. Grimaud and colleagues reported the blueshift of the water vibrational peaks of FTIR in the LiTFSI-based WiSE.[34] Pan and colleagues reported the blueshift of water peaks in Raman in the concentrated $LiNO_3$.[35] Grimaud and colleagues attributed their observed blueshift and the associated consolidated O–H bonds to the strong anion-proton interaction.[34] However, the electrons from anions as Lewis bases going into the antibonding orbitals of water as a Lewis acid would lower the bond strength.

We tentatively attribute the strengthened O–H bonds of water in the mixture WiSE of $ZnCl_2$ and LiCl to three factors. First, the swarming of cations and anions around water molecules prevents water molecules from forming a contiguous hydrogen bonding network—one primary factor that weakens the O–H bonds of water. Second, the presence of superhalides, for example, $[ZnCl_4]^{2-}$, seems to counterbalance the weakening impacts of hydrogen bonding on water. Third, Li-ions compete against Zn-ions to use water as ligands; thus, fewer hydrated Zn-ions involve in ZMA plating, and fewer free water molecules are released on the freshly plated surface of ZMA. This may mitigate hydrogen evolution.

To investigate whether atomic chloride ions have the same O–H strengthening effect as superhalides do in WiSE, we evaluated the O–H peaks in the concentrated aqueous LiCl solution by FSRS. Therein, the redder O–H stretch also vanishes gradually upon increasing the concentration due to the swarming effect of ions, but the bluer peak does not blueshift with the concentration going from 5 to 20 m (Figure S3c). Note that the O–H stretch of water in 30ZC10LC is 3481 cm^{-1}, higher than 3455 cm^{-1} in 20 m LiCl, which suggests that the gradual blueshifts in LiCl-$ZnCl_2$ WiSE is due to the increasing quantity of Zn–Cl superhalides. The more blueshift of the O–H stretch in water in the presence of concentrated superhalides, for example, $[ZnCl_4]^{2-}$, than in the presence of more Cl^- ions sheds light on the postulation that superhalides with stronger electron-donating ability seem to better stabilize water molecules in counteracting against the weakening effects.[36] The observed peak blueshift from 30ZC, 30ZC3LC, 30ZC5LC to 30ZC10LC (Figure 2C) should be attributed to the more presence of Zn–Cl superhalides and their aggregates.

FTIR spectra also reveal the influence of the LiCl addition on the O–H bonds of water in the mixture electrolytes (Figure S4a). A high concentration of $ZnCl_2$ in 30ZC solution changes the characteristic O–H stretch vibration from a broadband at 3242 to 3353 cm^{-1} in pure water to a relatively sharper and bluer peak centered around 3372 cm^{-1} in 30ZC. By adding LiCl, the O–H stretch further blueshifts to ~3394 cm^{-1} in 30ZC10LC. Notably, both FSRS and FTIR results demonstrate the consolidation of O–H bonds by adding LiCl as the co-salt.

The PDF studies associated with neutron total scattering were conducted to further investigate the atomic structure of different WiSE (Figure 2D). The weak peak located around 2 Å in the PDF profiles represents the superposition of the distances between Zn and O (d_{Zn-O}) and between Li and O (d_{Li-O}) in the mixture LiCl-$ZnCl_2$ WiSE electrolytes.[31,37] Upon increasing the LiCl concentration, this peak shifts to a smaller distance, which suggests the LiCl addition causes the Zn^{2+} hydration shell to be further incomplete (Figure 2C). Moreover, with increasing the LiCl concentration, the peak centered at 2.3 Å assigned to the distance between Zn and Cl (d_{Zn-Cl})[31] intensifies and moves to a higher value (Figure 2D). This suggests the formation of more Zn–Cl superhalides, for example, $[ZnCl_4]^{2-}$, at the expense of fewer hydrated Zn^{2+} ions and diminished interactions between Zn^{2+} and water molecules.

In summary, all Raman, FTIR, and PDF results demonstrate that the introduction of LiCl weakens the interaction between Zn^{2+} and water and promotes the formation of Zn–Cl superhalides, where the hydrogen bonding network is fragmented, and the O–H covalent bonds in water are strengthened. However, from 30ZC5LC to 30ZC10LC, the concentration of hydrated Zn^{2+} decreases, where according to the Nernst equation, the Zn plating/stripping potential goes down, as shown in Figure S5. A lower potential of Zn plating favors hydrogen evolution, which may explain the lower CE of 30ZC10LC than that of 30ZC5LC. In addition, the lowered conductivity of Zn^{2+} upon increasing the concentration of LiCl from 5 to 10 m should also contribute to the decreased reversibility of ZMA in 30ZC10LC electrolyte (Figure 1B), as the lower conductivity of Zn^{2+} causes a higher overpotential, which further lowers

the plating potential of ZMA, thus promoting the H_2 evolution.

2.2 | Simulation of the atomic structure of the LiCl-$ZnCl_2$ WiSE

To investigate the impacts of LiCl addition in the mixture electrolytes, we performed *ab initio* molecular dynamics (MD) simulations for various concentrations of LiCl mixed with 30ZC. To generate the initial atomic structures of these complex mixtures, we used a packing-optimization strategy of the molecular components (i.e., LiCl, $ZnCl_2$, and H_2O) that balances the short-range interactions such that the MD simulation is not disrupted, where each system contains 30 H_2O molecules. Next, we equilibrated the system for 20 picoseconds with a timestep of 1 femtosecond, where the total energy of the system gradually decreased and became stabilized after 3 picoseconds (Figure S6). As shown in Figure S7, the box of 30ZC comprises octahedral Zn^{2+} complex ions with H_2O and Cl^- as ligands, where the neighboring complexes are connected by bridging chloride ions, thus forming polynuclear aggregates. Additionally, many water molecules act as ligands to form various quasi-octahedral complexes from $[ZnCl(H_2O)_5]^+$ to $[ZnCl_5(H_2O)]^{3-}$. Similar agglomerates were also observed in the systems with LiCl added to 30ZC.

To understand the origin of the disparity in CE between the single and bi-salt WiSE, we compared the arrangement of waters in various salt concentrations (Figure 3A-C; Cl^- ions not shown). Interestingly, the number of hydrogen bonds between water molecules decreases from 20 for 30ZC to 14 for 30ZC10LC in the system. This corroborates the FSRS and FTIR results that the addition of LiCl to $ZnCl_2$ WiSE further disrupts the network of hydrogen bonding. Furthermore, the LiCl addition decreases the extent of Zn^{2+} hydration. In 30ZC5LC and 30ZC10LC, Li-ions capture 8 and 15 waters out of 30, respectively. Thus, the number of uncoordinated free water molecules decreases from 7 in 30ZC to four and 3 in 30ZC5LC and 30ZC10LC, respectively. Along this line, we also studied 10 m $ZnCl_2$ (10 ZC), and found the majority of Zn^{2+} ions form $ZnCl_2(H_2O)_2$ quasitetrahedral structures with 19 free water molecules (Figure S8). Having fewer free water molecules available in a system suggests a smaller activity of water and consequently a depressed potential of hydrogen evolution at the anode surface,[38] which is consistent with the experimental finding that bi-salt WiSE systems give rise to a higher CE than a single-salt 30ZC electrolyte.[38]

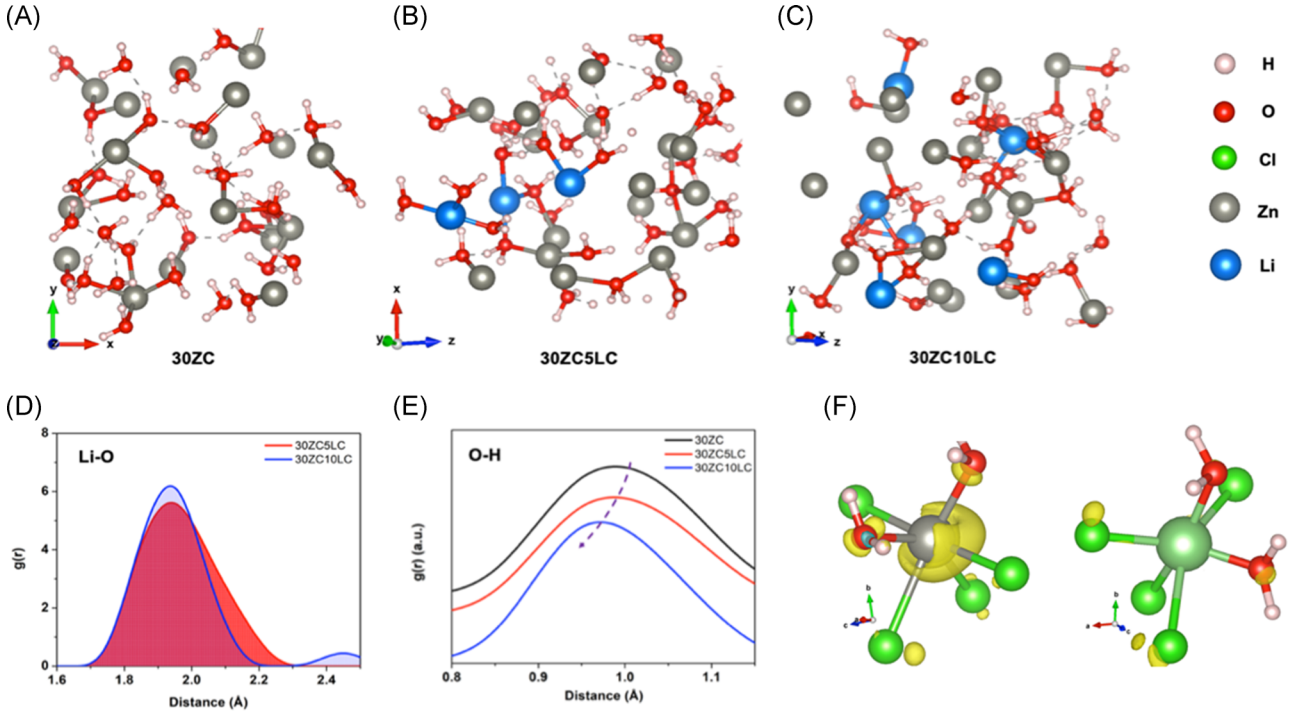

FIGURE 3 *Ab initio* molecular dynamics simulation studies. Snapshots of (A) 30ZC, (B) 30ZC5LC, (C) 30ZC10LC. Cl atoms are omitted to clarify the surrounding environment of Zn. Calculated radial distribution function profiles of (D) Li–O and (E) O–H pair for various concentrations. F, Charge density difference plots of extracted $ZnCl_4(H_2O)_2$ (left) and $LiCl_4(H_2O)_2$ (right) out of the entire simulation box where 10 extra electrons were introduced. Yellow isosurface represents electron accumulated regions compared with the pristine state. The isosurface level was set to 0.005 eV/Å

To compare the chemical environments of water quantitatively in these WiSE formulae, we plotted the radial distribution functions (RDFs) for different pairs over the entire virtue box. The Li–O RDF shows that Li-ions bind with water in a distance ranging from 1.7 to 2.2 Å in 30ZC5LC and 30ZC10LC (Figure 3D). For the O–H RDF, the peak bond length decreases from 0.99 to 0.96 Å upon LiCl addition (Figure 3E). This again validates the FSRS and FTIR results that the O–H bond in water is strengthened. By inspecting the box, the water molecules of the shortest O–H bonds are those bound on Zn/Li centers without any hydrogen bonds around. The water molecules of intermediate O–H bond length are affected by hydrogen bonds, which makes the bond length slightly longer. These results imply that the numbers of free waters and hydrogen bonds are descriptors to understand water's reactivity, particularly its cathodic stability, during Zn plating/stripping.

To probe the cathodic stability of water in LiCl-$ZnCl_2$ WiSE, we examined the mapping of charge difference in one snapshot of the 30ZC5LC model when it is artificially reduced with 10 extra electrons added (with a charge compensating positive background charge), which mimics the reduction of a quarter of the Zn^{2+} complex ions in the virtual box. The electron density changes on representative Zn^{2+}-containing and Li^{+}-containing complex ions are extracted from this calculation, as shown in Figure 3F. The extra electrons accumulate (yellow isosurface region) on the Zn^{2+} ions and on the oxygen atoms of the water molecules that coordinate Zn^{2+}, which renders the reduction of the ligand water molecules viable. However, few extra electrons reside on Li-ions or its coordinating water molecules; thus, these Li-ion-binding water molecules are less likely to be reduced. This is consistent with the enhanced CE results upon LiCl addition.

2.3 | The cycling stability of ZMA in WiSEs

Cycling at a large capacity and a high current density for a long period of time has remained a challenge for ZMA in aqueous electrolytes due to dendrite formation. In most prior studies, the areal capacity is no higher than 1 mAh cm^{-2}, and the cycling duration is no more than 1000 hours (Table S2). Indeed, the use of 3D current collectors or Zn powder anode lowers the local current density, which decreases the operation overpotential of ZMA and promotes cycling stability[18,39]; however, the larger surface area also endows ZMA with more active sites to react with water, which may compromise the CE to a certain extent.

Here, we investigated the cycling stability of ZMA in the $ZnCl_2$ and $ZnCl_2$-LiCl mixture electrolytes. In symmetrical cells with ZMA as the working and counter electrodes, both electrolytes of 30ZC and 30ZC5LC exhibit stable GCD cycling at 1 mA cm^{-2} with a moderate areal capacity of 1 mAh cm^{-2} for 2000 hours, where the overpotentials are only 16 and 13 mV, respectively (Figure 4A). To stress the stability of ZMA, we increased the areal capacity to 4 mAh cm^{-2} for each cycle and raised the current density to 2 mA cm^{-2} (C/2). Under these "harsh" conditions, the symmetrical Zn cells with the 30ZC electrolyte short-circuited after cycling for 500 hours (Figure 4B, black, and Figure S9). In contrast, the cell containing 30ZC5LC displays excellent stability, where the GCD profiles show no obvious potential fluctuation over 4000 hours (Figure 4B, red). To the best of our knowledge, such cycling stability exceeds most ZMA in aqueous electrolytes reported so far (Table S2).

Figures 4C,D and S10 display the scanning electron microscopy images of ZMA in 30ZC and 30ZC5LC electrolytes after 100 cycles with a capacity of 4 mAh cm^{-2} at 2 mA cm^{-2}, where the former displays a mossy and dendritic morphology, whereas the latter exhibits a uniform and compact morphology without any dendrite formation. It should be noted that the smooth and compact morphology for Zn is conducive to promoted reversibility for the Zn anode as the smooth surface exposes fewer sites of ZMA to react with water than the mossy morphology.

The stability performance disparity between 30ZC5LC and 30ZC electrolytes can be attributed to the formation of a screening layer of Li-ions at the surface of ZMA, where Li-ions do not get reduced, and, thus, electrostatically shield asperities and perturbations to prevent runaway dendrite growth (Figure S11). Such a cation layer eliminates the ion depletion zone in Sand's model, where the depletion zone is known responsible for the dendrite growth during metal plating.[18,39] Zhang et al. reported that the addition of Cs^{+} promotes plating stability of lithium[40]—an analogue phenomenon. This effect of the additives has also been demonstrated in other research studies for increasing the stability of metal anodes.[40-43] However, it should be noted that the difference between this study and the previous studies is the dosage of the additives. Herein, we added a considerable amount of LiCl, where LiCl is a bifunctional additive that not only suppresses the dendrite formation but also effectively increases the reversibility of Zn anode by minimizing the number of free water molecules and downsizing the hydration shells of Zn^{2+}.

2.4 | The applicability of LiCl-$ZnCl_2$ WiSE in full cells

We investigated the applicability of the LiCl-$ZnCl_2$ WiSE in full cells with vanadium oxide and lithium manganate

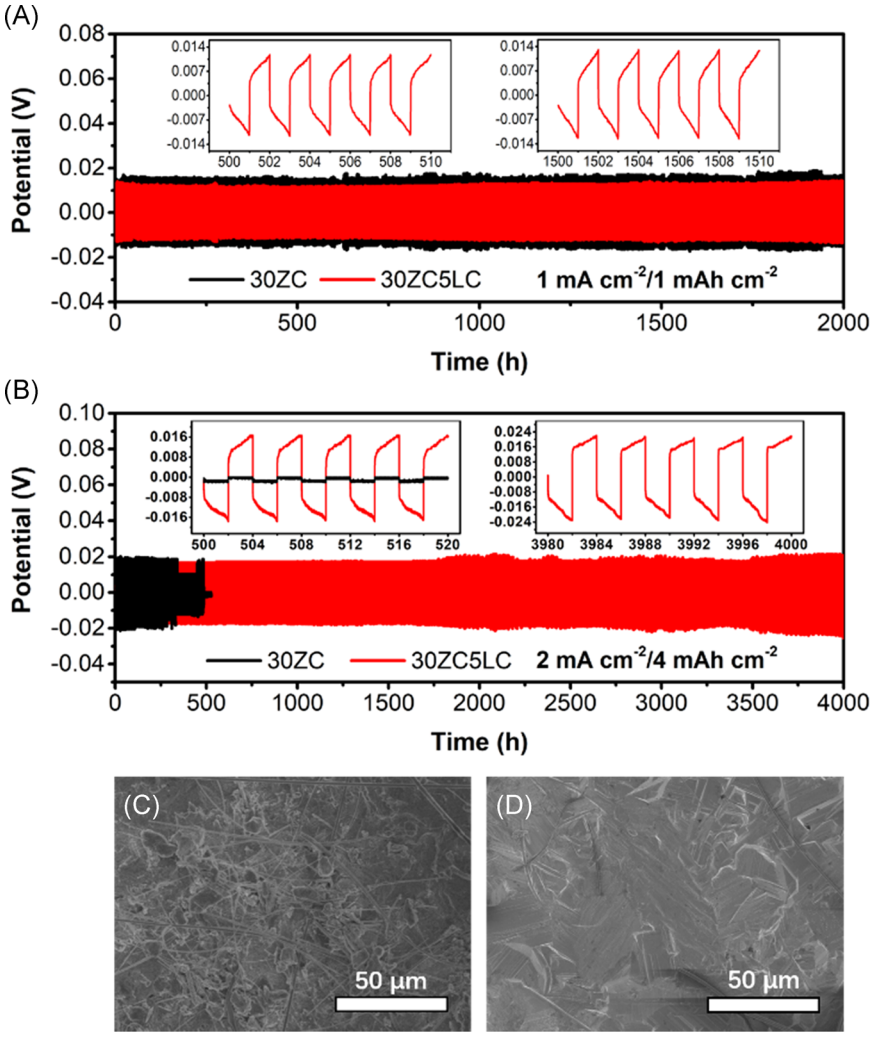

FIGURE 4 The stability performance of the zinc-metal anode in 30ZC and 30ZC5LC electrolytes. The GCD potential profiles of Zn plating/stripping in 30ZC and 30ZC5LC in Zn||Zn symmetrical cells at (A) 1 mA cm^{-2} for 1 hour and (B) 2 mA cm^{-2} for 2 hours. The scanning electron microscopy images of the plated Zn after 100 cycles with a capacity of 4 mAh cm^{-2} at 2 mA cm^{-2} in (C) 30ZC and (D) 30ZC5LC electrolytes

as the cathodes, respectively. The bilayered $V_2O_5{\cdot}H_2O$ cathode has been widely studied as a cathode for aqueous ZMBs.[4] The characterization results of $V_2O_5{\cdot}H_2O$ are shown in Figure S12. In half cells, $V_2O_5{\cdot}H_2O$ was cycled for more than 1000 and 5000 cycles at 2 A g^{-1} in 30ZC and $ZnCl_2$-LiCl WiSE, respectively, which shows its high stability in $ZnCl_2$-based WiSE (Figure S13). In the $V_2O_5{\cdot}H_2O$||30ZC5LC||Zn full cells, where the ZMA/$V_2O_5{\cdot}H_2O$ N/P mass ratio was set to be 1.2, the $V_2O_5{\cdot}H_2O$ cathode displays more than 500 cycles at 2 A g^{-1} in 30ZC5LC (Figure S14). The 30ZC electrolyte was also employed as a controlled electrolyte, where its full cell starts to lose capacity rapidly after 280 cycles at 2 A g^{-1} (Figure S14). Hence, 30ZC5LC improves the reversibility and stability of ZMA, which promotes the cycle life of full cells. By considering the total mass of ZMA (the initial mass and the mass produced from the cycling as the CE of the full cell is not 100%) as well as the capacity fading, there is 22.2% of original ZMA remaining after 500 cycles in the 30ZC5LC electrolyte. Conversion from 100% to 22.2% in 500 cycles corresponds to an average CE of 99.7% for ZMA in each cycle. In contrast, the calculated CE for ZMA based on the cycling data of the full cell with the 30ZC electrolyte is only 99.2%. The $V_2O_5{\cdot}H_2O$||30ZC5LC||Zn full cell delivered a long cycling life of 2500 cycles at 5 A g^{-1} (Figure S14), which corresponds to a CE of more than 99.9%.

The mixture electrolyte also makes it viable to pair ZMA with the commercial cathode of $LiMn_2O_4$ in a hybrid ZMB (see characterization results of $LiMn_2O_4$ in Figure S15). Note that the concentration of LiCl in the electrolyte may affect the mass ratio between the electrolyte and the electrodes in practical cells. Nevertheless, the high saturation concentrations of $ZnCl_2$ (31 m in water) and LiCl (20 m in water) will benefit the $LiMn_2O_4$||Zn hybrid cell system to achieve a high energy density. We selected 30ZC10LC WiSE as the electrolyte, as the $LiMn_2O_4$||Zn cell shows better cycling stability in 30ZC10LC WiSE than in 30ZC5LC WiSE (Figure S16). The stability of the Zn anode in 30ZC10LC was also studied, which delivered a stable cyclability for 4000 hours without obvious potential fluctuations at

2 mAh cm^{-2}. The $LiMn_2O_4$||30ZC10LC||Zn full cells, where the *N*/*P* mass ratio of ZMA to $LiMn_2O_4$ was only 0.6, are able to show more than 1500 cycles at 0.48 A g^{-1}, corresponding to a CE of 99.7% for the Zn anode in each cycle (Figure S17). Considering the mass loading of $LiMn_2O_4$ is ~6 to 7 mg cm^{-2}, the current rates of 60 and 480 mA g^{-1} correspond to the current density of 0.36 to 0.42 and 2.88 to 3.36 mA cm^{-2}, respectively. Thus, the $LiMn_2O_4$||Zn full cell with an *N*/*P* mass ratio of 0.6 shows more than 180 and 1500 cycles at a current density of 0.36 to 0.42 and 2.88 to 3.36 mA cm^{-2}, respectively. Therefore, the above excellent performance of ZMBs with $V_2O_5{\cdot}H_2O$ and $LiMn_2O_4$ as the cathodes demonstrate the practical applicability of the $ZnCl_2$-LiCl mixture WiSE electrolytes, which may render the low-cost and high-performance aqueous ZMB practically viable.

3 | CONCLUSIONS

By investigating the LiCl-$ZnCl_2$ mixture concentrated electrolyte, advanced characterization and complementary MD simulation collectively demonstrate that hydrogen bonding in water is detrimental to the reversibility of ZMA. Hydrogen bonding of water can serve as a descriptor for ZMA's cycling irreversibility. Disrupting the hydrogen bonding network by soliciting water molecules in coordination shells can counteract the weakening effect of hydrogen bonding. With fewer hydrogen bondings, water molecules exhibit a shortened and stiffened O–H covalent bond, where we found these properties are correlated to higher CE of ZMA plating-stripping. The higher CE of ZMA can be attributed to better cathodic stability of water; thus, water is more inert in the presence of both LiCl and concentrated $ZnCl_2$. We also found that water molecules coordinating Zn^{2+} are more likely to be reduced than those coordinating Li^+. As a result, the addition of LiCl increases the CE of ZMA near unity at 1 mA cm^{-2}. The mixture electrolyte also endows ZMA with excellent stability and dendrite-free morphology. Finally, the LiCl-$ZnCl_2$ WiSE electrolyte manifests applicability in full cells with a limited mass of ZMA. This cost-effective LiCl-$ZnCl_2$ WiSE offers a new opportunity to realize practical applications of high-performance and low-cost aqueous ZMBs.

ACKNOWLEDGMENTS

XJ thanks Oregon State University for AID program support. J-XJ thanks the financial support from the National Natural Science Foundation of China (21574077 and 21304055), 111 project (B14041), the Fundamental Research Funds for the Central Universities (GK201801001). CZ is supported by a fellowship from the China Scholarship Council (201706870033) CF is grateful to the U.S. National Science Foundation CAREER grant (CHE-1455353) for the support of the femtosecond stimulated Raman instrumentation and the NSF MRI grant (DMR-1920368) for additional support.

CONFLICT OF INTEREST

The authors declare no conflict of interest. [Correction added on 15 June 2021, after first online publication: Conflict of Interest section has been added.]

ORCID

Chong Fang https://orcid.org/0000-0002-8879-1825
Xiulei Ji http://orcid.org/0000-0002-4649-9594

REFERENCES

1. Kundu D, Adams BD, Duffort V, Vajargah SH, Nazar LF. A high-capacity and long-life aqueous rechargeable zinc battery using a metal oxide intercalation cathode. *Nat Energy*. 2016;1:16119.
2. Wu M, Zhang G, Hu Y, et al. Graphitic-shell encapsulated FeNi alloy/nitride nanocrystals on biomass-derived N-doped carbon as an efficient electrocatalyst for rechargeable Zn-air battery. *Carbon Energy*. 2021;31:176-187.
3. Zhang K, Zhang Y, Zhang Q, et al. Metal-organic framework-derived Fe/Cu-substituted Co nanoparticles embedded in CNTs-grafted carbon polyhedron for Zn-air batteries. *Carbon Energy*. 2020;2:283-293.
4. Kundu D, Hosseini VS, Wan L, Adams B, Prendergast D, Nazar LF. Aqueous vs. nonaqueous Zn-ion batteries: consequences of the desolvation penalty at the interface. *Energy Environ Sci*. 2018;11:881-892.
5. Jiang H, Ji X. Counter-ion insertion of chloride in Mn_3O_4 as cathode for dual-ion batteries: a new mechanism of electrosynthesis for reversible anion storage. *Carbon Energy*. 2020;2:437-442.
6. Wang P, Shi X, Wu Z, Guo S, Zhou J, Liang S. Layered hydrated vanadium oxide as highly reversible intercalation cathode for aqueous Zn-ion batteries. *Carbon Energy*. 2020;2:294-301.
7. Zhang L, Chen L, Zhou X, Liu Z. Towards high-voltage aqueous metal-ion batteries beyond 1.5 V: the zinc/zinc hexacyanoferrate system. *Adv Energy Mater*. 2015;5:1400930.
8. Wu X, Xu Y, Zhang C, et al. Reverse dual-ion battery via a $ZnCl_2$ water-in-salt electrolyte. *J Am Chem Soc*. 2019;141:6338-6344.
9. Shi H-Y, Ye Y-J, Liu K, Song Y, Sun X. A long-cycle-life self-doped polyaniline cathode for rechargeable aqueous zinc batteries. *Angew Chem Int Ed*. 2018;57:16359-16363.
10. Xiao B. Intercalated water in aqueous batteries. *Carbon Energy*. 2020;2:251-264.
11. Wang F, Borodin O, Gao T, et al. Highly reversible zinc metal anode for aqueous batteries. *Nat Mater*. 2018;17:543-549.
12. Dong W, Shi J-L, Wang T-S, Yin Y-X, Wang C-R, Guo Y-G. 3D zinc@carbon fiber composite framework anode for aqueous Zn–MnO_2 batteries. *RSC Adv*. 2018;8:19157-19163.
13. Kang Z, Wu C, Dong L, et al. 3D porous copper skeleton supported zinc anode toward high capacity and long cycle life zinc ion batteries. *ACS Sustainable Chem Eng*. 2019;7:3364-3371.

14. Wang Z, Huang J, Guo Z, et al. A metal-organic framework host for highly reversible dendrite-free zinc metal anodes. *Joule*. 2019;3:1289-1300.
15. Wang L-P, Li N-W, Wang T-S, Yin Y-X, Guo Y-G, Wang C-R. Conductive graphite fiber as a stable host for zinc metal anodes. *Electrochim Acta*. 2017;244:172-177.
16. Zheng J, Zhao Q, Tang T, et al. Reversible epitaxial electrodeposition of metals in battery anodes. *Science*. 2019;366:645-648.
17. Kang L, Cui M, Jiang F, et al. Nanoporous $CaCO_3$ coatings enabled uniform Zn stripping/plating for long-life zinc rechargeable aqueous batteries. *Adv Energy Mater*. 2018;8:1801090.
18. Li G, Liu Z, Huang Q, et al. Stable metal battery anodes enabled by polyethylenimine sponge hosts by way of electrokinetic effects. *Nat Energy*. 2018;3:1076-1083.
19. Zhao Z, Zhao J, Hu Z, et al. Long-life and deeply rechargeable aqueous Zn anodes enabled by a multifunctional brightener-inspired interphase. *Energy Environ Sci*. 2019;12:1938-1949.
20. Xie X, Liang S, Gao J, et al. Manipulating the ion-transfer kinetics and interface stability for high-performance zinc metal anodes. *Energy Environ Sci*. 2020;13:503-510.
21. Yang H, Chang Z, Qiao Y, et al. Constructing a supersaturated electrolyte front surface for stable rechargeable aqueous zinc batteries. *Angew Chem Int Ed*. 2020;59:9377-9381.
22. Sun KEK, Hoang TKA, Doan TNL, Yu Y, Chen P. Highly sustainable zinc anodes for a rechargeable hybrid aqueous battery. *Chem Eur J*. 2018;24:1667-1673.
23. González MA, Trócoli R, Pavlovic I, Barriga C, La Mantia F. Layered double hydroxides as a suitable substrate to improve the efficiency of Zn anode in neutral pH Zn-ion batteries. *Electrochem commun*. 2016;68:1-4.
24. Zhang C, Holoubek J, Wu X, et al. A $ZnCl_2$ water-in-salt electrolyte for a reversible Zn metal anode. *Chem Commun*. 2018;54:14097-14099.
25. Adams BD, Zheng J, Ren X, Xu W, Zhang J-G. Accurate determination of Coulombic efficiency for lithium metal anodes and lithium metal batteries. *Adv Energy Mater*. 2018;8:1702097.
26. Wu X, Markir A, Xu Y, et al. A rechargeable battery with an iron metal anode. *Adv Funct Mater*. 2019;29:1900911.
27. Huang J, Wang Z, Hou M, et al. Polyaniline-intercalated manganese dioxide nanolayers as a high-performance cathode material for an aqueous zinc-ion battery. *Nat Commun*. 2018;9:2906.
28. Wu X, Li Y, Li C, et al. The electrochemical performance improvement of $LiMn_2O_4$/Zn based on zinc foil as the current collector and thiourea as an electrolyte additive. *J Power Sources*. 2015;300:453-459.
29. Yamaguchi T, Hayashi S, Ohtaki H. X-ray diffraction and Raman studies of zinc(II) chloride hydrate melts, $ZnCl_2{\cdot}RH_2O$ ($R = 1.8$, 2.5, 3.0, 4.0, and 6.2). *J Phys Chem*. 1989;93:2620-2625.
30. Kanno H, Hiraishi J. Raman spectroscopic study of glassy aqueous zinc halide solutions. *J Raman Spectrosc*. 1980;9:85-89.
31. Wilcox RJ, Losey BP, Folmer JCW, Martin JD, Zeller M, Sommer R. Crystalline and liquid structure of zinc chloride trihydrate: a unique ionic liquid. *Inorg Chem*. 2015;54:1109-1119.
32. Chen C-Y, Matsumoto K, Kubota K, Hagiwara R, Xu Q. A room-temperature molten hydrate electrolyte for rechargeable zinc–air batteries. *Adv Energy Mater*. 2019;9:1900196.
33. Hong JJ, Zhu L, Chen C, et al. A dual plating battery with the iodine/$[ZnI_x(OH_2)_{4-X}]^{2-X}$ cathode. *Angew Chem Int Ed*. 2019;58:15910-15915.
34. Dubouis N, Lemaire P, Mirvaux B, Salager E, Deschamps M, Grimaud A. The role of the hydrogen evolution reaction in the solid–electrolyte interphase formation mechanism for "Water-in-Salt" electrolytes. *Energy Environ Sci*. 2018;11:3491-3499.
35. Zheng J, Tan G, Shan P, et al. Understanding thermodynamic and kinetic contributions in expanding the stability window of aqueous electrolytes. *Chem*. 2018;4:2872-2882.
36. Lin R-G, Xu G, Lu G, Wang MS, Li PX, Guo GC. Photochromic hybrid containing in situ-generated benzyl viologen and novel trinuclear $[Bi_3Cl_{14}]^{5-}$: improved photoresponsive behavior by the π-π interactions and size effect of inorganic oligomer. *Inorg Chem*. 2014;53:5538-5545.
37. Mason PE, Ansell S, Neilson GW, Rempe SB. Neutron scattering studies of the hydration structure of Li^+. *J Phys Chem B*. 2015;119:2003-2009.
38. Suo L, Borodin O, Gao T, et al. "Water-in-Salt" electrolyte enables high-voltage aqueous lithium-ion chemistries. *Science*. 2015;350:938-943.
39. Sand HJS. On the concentration at the electrodes in a solution, with special reference to the liberation of hydrogen by electrolysis of a mixture of copper sulphate and sulphuric acid. *Philos Mag*. 1901;1:45-79.
40. Ding F, Xu W, Graff GL, et al. Dendrite-free lithium deposition via self-healing electrostatic shield mechanism. *J Am Chem Soc*. 2013;135:4450-4456.
41. Yu L, Chen S, Lee H, et al. A localized high-concentration electrolyte with optimized solvents and lithium difluoro(oxalate)borate additive for stable lithium metal batteries. *ACS Energy Lett*. 2018;3:2059-2067.
42. Dai H, Xi K, Liu X, Lai C, Zhang S. Cationic surfactant-based electrolyte additives for uniform lithium deposition via lithiophobic repulsion mechanisms. *J Am Chem Soc*. 2018;140:17515-17521.
43. Chang G, Liu S, Fu Y, et al. Inhibition role of trace metal ion additives on zinc dendrites during plating and striping processes. *Adv Mater Interfaces*. 2019;6:1901358.

SUPPORTING INFORMATION

Additional supporting information may be found online in the Supporting Information section.

How to cite this article: Zhang C, Shin W, Zhu L, et al. The electrolyte comprising more robust water and superhalides transforms Zn-metal anode reversibly and dendrite-free. *Carbon Energy*. 2021;3:339–348. https://doi.org/10.1002/cey2.70